Research Article

Three Decades of Changes in the Urban Heat Island Effect in Denver, Colorado, Revealed by Landsat

Sadia Islam Ritu[1] and Bruce Millett[2,*]

[1] Department of Geography and Environmental Studies, Texas State University, San Marcos, Texas, USA; ghw31@txstate.edu

[2] Department of Geography and Geospatial Sciences, South Dakota State University, Brookings, South Dakota, USA; bruce.millett@sdstate.edu

[*] Corresponding Author: bruce.millett@sdstate.edu; +1-605-688-4833.

Abstract: Rapid urbanization has imposed negative environmental impacts and contributed to global climate change on multiple scales. The urban heat island (UHI) is directly caused by urban expansion, dramatically increasing land surface temperature (LST). Despite the growing concern about the UHI in Denver, Colorado, few studies among the existing literature have addressed this issue. This study used United States Geological Survey (USGS) Landsat 5, 7, and 8 analysis-ready data (ARD) to characterize land cover changes and UHI in Denver for three decades (e.g., 1990, 2000, 2010, and 2020). Land surface temperature was derived from USGS Landsat Collection 2 ARD for twelve dates across summer, fall, and winter seasons in 1990, 2000, 2010, and 2020, and analyzed on both seasonal and annual scales. Land cover change (LCC) analysis detected a 13% increase in developed land cover and a 12% decrease in cropland and grass/shrubs from 1990 to 2020. The relationship between land cover and LST was modeled using ordinary least squares (OLS) and geographically weighted regression (GWR) analysis between land cover indices—e.g., the normalized difference vegetation index (NDVI), two-band enhanced vegetation index (EVI2), urban index (UI), and LST. The results from the regression models showed seasonal variability, spatiotemporal variations, and other underlying factors affecting the bivariate correlations. Finally, the seasonal and annual distribution and variation of UHI intensity were measured, and it was identified that the mean annual UHI intensity in 2020 was 1°C higher than that recorded in 1990, which illustrated a consistent spatial distribution throughout downtown Denver and the central areas of the city, while the intensity of UHI represented a more scattered distribution in the non-urban areas. The methods applied in this study can serve as a model for future research on other cities, and the findings can be used to inform sustainable urban planning and to mitigate the effects of UHI in Denver.

Keywords: land surface temperature, urban heat island, surface reflectance, ordinary least squares, geographically weighted regression

Academic Editor: Mohamed Aly
Received: 1 July 2025
Revised: 24 September 2025; 6 October 2025
Accepted: 10 October 2025
Published: 24 October 2025

1. Introduction

Rapid urbanization has profoundly transformed landscapes worldwide over the past few decades (UN, 2018). Currently, more than 50% of the global population resides in cities, a proportion projected to exceed 60% by 2030 (Keyvan *et al*., 2021). Urban growth alters land cover and surface energy balances through the expansion of impervious and built-up surfaces, fundamentally reshaping the urban environment. These processes are central to land cover change (LCC) studies, as urban expansion is closely linked to increasing imperviousness.

One of the most significant consequences of urban land use/land cover (LULC) change is the modification of land surface temperature (LST), which is also influenced by urban heat balance and climate change (Yuvaraj, 2020). LST reflects energy fluxes between the atmosphere and the land surface and provides an important measure of atmosphere–surface interactions (Zhengming & Dozier, 1996; Liu & Weng, 2009). Consequently, the spatial and temporal patterns of LST reveal variations in climate, land surface properties,

Citation: Ritu, S. I., & Millett, B. (2025). Three decades of changes in the urban heat island effect in Denver, Colorado, revealed by Landsat. *Journal of Earth Observation and Geospatial Applications*, *1*(1), 64–82. DOI: https://doi.org/10.65372/e3fq4y36

and urban development (Yuvaraj, 2020). Understanding the urban thermal environment therefore requires examining key factors such as LST, land cover, and solar radiation (Aguiar & Gonçalves, 2002; Liu & Weng, 2009).

The urban heat island (UHI) effect—defined as the increase of surface temperatures in urban areas relative to surrounding rural zones—arises from reduced albedo, limited evapotranspiration, and intensified anthropogenic heat emissions (Voogt & Oke, 2003). LST differences between urban and rural areas are used to quantify UHI intensity (George *et al*., 2022). Advances in thermal remote sensing have enabled extensive research on surface urban heat islands (SUHI), providing spatially and temporally consistent observations of LST (Voogt & Oke, 2003). For example, comparative analyses of metropolitan regions such as Atlanta and Minneapolis demonstrated that variations in LST between urban and adjacent non-urban areas reflect differences in UHI intensity and landscape thermal properties (George *et al*., 2022).

Currently, satellite-based thermal infrared remote sensing provides the most effective means of investigating spatial and temporal variations in LST (Yuvaraj, 2020). This technology is indispensable for understanding the complexities of urban thermal environments and surface–atmosphere energy exchanges, due to its ability to provide synoptic, consistent, and long-term records (George *et al*., 2022).

Spatiotemporal modeling of the UHI effect using Landsat TM and ETM+ imagery has shown that early studies primarily focused on the relationship between land cover composition, particularly vegetation abundance, and LST (Buyantuyev *et al*., 2010; Frey *et al.,* 2007; Weng *et al*., 2006). Because ground station data are sparse and unevenly distributed, they are insufficient for characterizing the spatial patterns of UHIs in a large area (George *et al*., 2022). Recent studies have moved beyond quantifying total vegetation cover to examine the influence of vegetation patch size, distribution, and configuration on LST (Cao *et al.,*2010; Peng *et al*., 2018; Yue *et al.,* 2007). Additional research has also investigated the relationship between landscape heterogeneity and variations in LST zones (Liu & Weng, 2009).

UHI intensity (UHII) is commonly measured as the LST difference between urban pixels and surrounding non-urban reference areas (Voogt & Oke, 2003; Xian, 2008; Imhoff *et al*., 2010; Clinton & Gong, 2013), with remote sensing providing the most effective means for capturing these differences (Streutker, 2002). Assessments of surface UHI typically focus on mapping UHII and its spatial distribution at a given time using remote sensing data integrated with land cover information (George *et al*., 2022). Urban footprints are often defined based on contiguous built-up areas, beginning with the central business district (CBD) and expanding outward (Harald *et al*., 2020; Richard *et al*., 2022). For example, Richard *et al*. (2022) used 8-day MODIS Aqua MYD11A2 composites (1 km resolution) to quantify UHI trends from 2003 to 2019, applying a 10 km buffer around urban boundaries to compare urban and surrounding non-urban LST. Their analysis further examined diurnal and nocturnal annual mean LST trends in six climate-diverse cities—continental (Beijing), temperate (Mexico City and Santiago), and arid (Cairo, Hyderabad, and Riyadh) using 1 km MODIS data (2003–2019). These methods highlight how thermal remote sensing can identify urban hotspots and support the design of targeted heat mitigation strategies (George *et al*., 2022).

Denver consistently ranks among the U.S. cities with the most intense UHI effects, placing third out of 60 cities in one national assessment (Kenward *et al*., 2014). Over the past decade, the city has exhibited an average urban–rural temperature difference of approximately 2.5 °C (4.9 °F), with more than 26 days each year exceeding 32 °C (90 °F). Rapid urbanization, population growth, and declining vegetation cover have intensified these effects. High-rise buildings, dark roofing, and impervious pavements exacerbate heat retention by reducing nighttime cooling and enhancing radiative and turbulent heat transfer (Davis, 2021). Despite these severe conditions, Denver has not been extensively studied using long-term remote sensing approaches, leaving gaps in understanding the role of land cover change in shaping UHI intensity.

This study addresses this gap by examining three decades (1990–2020) of satellite-derived data to investigate the relationship between LCC, LST, and UHI intensity in Denver. Using Landsat Analysis Ready Data (ARD), we quantified changes in land cover composition and assessed the spatial and temporal dynamics of LST. UHI intensity was evaluated by comparing urban pixel temperatures with the mean LST of non-urban buffer zones (5 km and 10 km). The analysis reveals extensive urban expansion over the study period and demonstrates its direct influence on surface temperature patterns. The study highlights the broader significance of understanding how long-term land cover dynamics contribute to UHI intensity in Denver. By integrating remote sensing with spatial analysis, this study provides valuable insights into how urban growth, loss of vegetation, and rising surface temperatures are connected. These findings provide an important foundation for guiding sustainable urban planning, promoting green infrastructure, and developing climate adaptation strategies to help reduce UHI impacts in rapidly growing cities.

2. Study Area and Data

2.1. Study Area

Denver is situated between the Rocky Mountains to the west and the High Plains to the east, at 39.74°N latitude and 104.99°W longitude (Figure 1). The city lies at an elevation of approximately 1,609 m above sea level, earning it the title "Mile High City." This elevation, combined with its mid-latitude location, produces a semi-arid climate characterized by mild winters, dry summers, and low relative humidity. These conditions not only shape local thermal dynamics but also amplify the UHI effect by reducing evaporative cooling potential and intensifying heat retention in built-up areas.

Denver is one of the fastest-growing metropolitan regions in the United States, with a population of 2.9 million that has expanded more rapidly than the national average (World Report, 2019). Rapid urbanization, coupled with the city's unique geographic and climatic context, makes Denver especially vulnerable to UHI effects. Between 2001 and 2016, the city underwent a net land cover change of 32.3 km², with substantial increases in medium and high-intensity development (MRLC, 2016). According to the National Land Cover Database, urban land is classified by imperviousness: high intensity (80–100%), medium intensity (50–79%), low intensity (20–49%), and open space (<20%) (Homer *et al*., 2020). Over this period, Denver County experienced an 8.05% change in land cover, including a gain of 16.9 km² in developed land and 11.91 km² in impervious surfaces. Grassland and cropland were the primary land cover types lost, converted into urban development.

Together, Denver's high elevation, semi-arid climate, and rapid urban expansion provide a unique setting for investigating UHI intensity and its drivers. These characteristics not only distinguish Denver from other U.S. cities but also highlight the need for long-term monitoring of land cover and temperature dynamics to better understand and mitigate the city's urban heat risks.

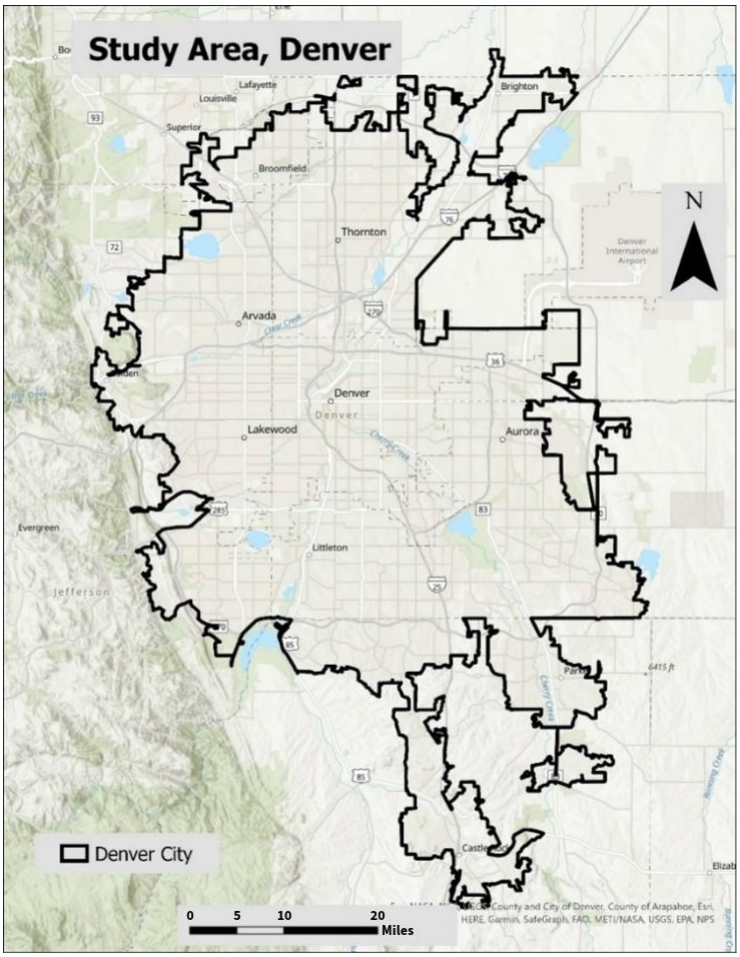

Figure 1. Map of the study area, Denver (Reprojected to NAD 1983 UTM Zone 13N).

2.2. Land Cover Data

Land cover change from 1990 to 2020 was examined using the Land Change Monitoring, Assessment, and Projection (LCMAP) dataset, obtained from the USGS Earth Explorer platform (Table 1). LCMAP provides annual land cover maps of the conterminous United States, classified into eight categories: Developed, Cropland, Grass/Shrub, Tree Cover, Wetland, Water, Ice/Snow, and Barren. These classes are based primarily on the Anderson Level I classification scheme (Anderson *et al*., 1976). For this study, land cover maps from the USGS LCMAP Collection 1 products were used directly for analysis, with a subset of the Denver metropolitan area. The permanent ice/snow class was excluded because it is not found in the study area; instead, seven of the eight land cover classes were used. The LCMAP product has an overall accuracy of 82.5%, validated through 25,000 randomly distributed reference samples annotated using Google Earth (Stephen *et al*., 2021).

Table 1. Necessary data for the study. Data source: U.S. Geological Survey (USGS). Projection: NAD 1983 UTM Zone 13N.

Data/ Product	Data Source	Years	Version	Resolution
Shapefile	TIGER Data Product			
LCMAP	USGS	1990	CCDC V 1.3	30 x 30 m
		2000		
		2010		
		2020		
Surface Reflectance (SR)	USGS	1990	Landsat C2 U.S. (ARD)	30 x 30 m
		2000	Landsat 5, 7 and 8	
		2010		
		2020		
Surface Temperature (ST)	USGS	1990	Landsat C2 U.S. (ARD)	30 x 30 m
		2000	(Landsat 5,7 and 8)	
		2010		
		2020		

2.3. Surface Reflectance Data

To minimize atmospheric influences on spectral measurements, Landsat surface reflectance products were employed. These products incorporate corrections for atmospheric aerosols, gases, and water vapor, thereby providing consistent geophysical and biophysical parameters across sensors and time periods (Dwyer *et al*., 2018). The use of surface reflectance data ensures the comparability of multi-temporal analyses of vegetation indices and land cover.

2.4. Land Surface Temperature Data

Land surface temperature was derived from the thermal bands of Landsat sensors. For historical observations, LST was extracted from band 6 of the Landsat 5 Thematic Mapper (TM). For recent years, LST was retrieved from band 10 of the Thermal Infrared Sensor (TIRS) onboard Landsat 8. These datasets enabled consistent estimation of spatial and temporal variations in LST over the 30-year study period.

3. Methods

This study followed a prototype workflow adapted from Xian *et al*. (2021). Land cover maps were generated from LCMAP data using ArcGIS Pro. Vegetation and urban indices, including the enhanced vegetation index 2 (EVI2), normalized difference vegetation index (NDVI), and urban index (UI), were derived from Landsat surface reflectance products. These indices were calculated using the Map Algebra function in the Spatial Analyst extension of ArcGIS Pro.

LST was calculated through raster-based map algebra operations using the Raster Calculator. To support statistical analysis, 800 sample points were generated through random sampling in ArcGIS Pro, and values of EVI2, NDVI, UI, and LST were extracted from the corresponding raster layers.

Ordinary least squares (OLS) regression and geographically weighted regression (GWR) were applied to assess spatial and temporal relationships between land cover indices and LST. Non-urban reference buffers were delineated using the Proximity Analysis tool, and zonal statistics were used to summarize mean conditions within these buffers. Urban heat island intensity was then computed as the difference between mean non-urban buffer temperatures and urban pixel temperatures, derived using Map Algebra in ArcGIS Pro (Figure 2).

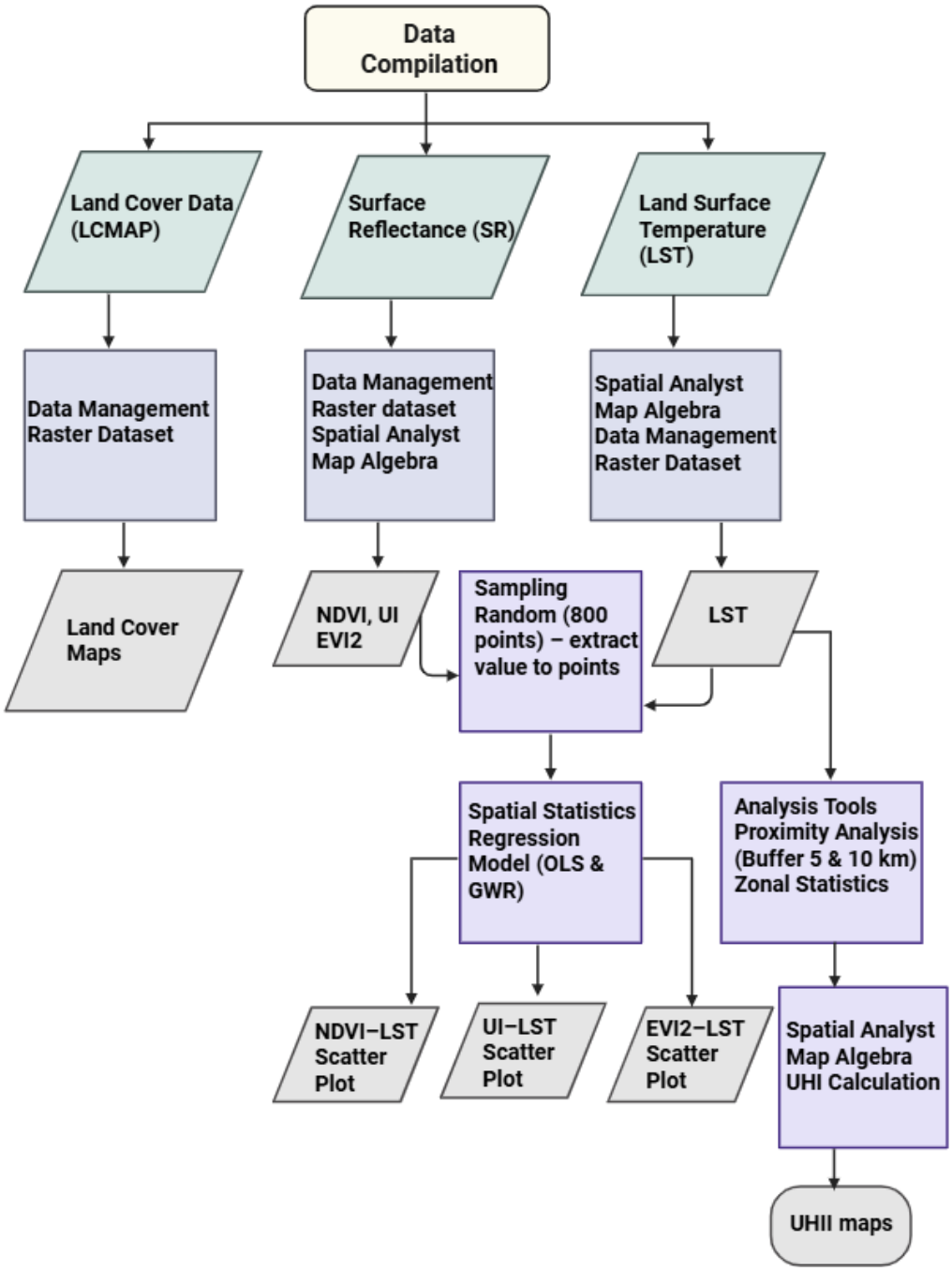

Figure 2. Workflow diagram.

3.1. Land Cover Change Analysis

The urban land cover map was derived from the LCMAP, which has eight primary land cover classes. LCMAPs from different years examined the changes in land cover over 30 years (e.g., from agricultural and rural land cover to developed impervious surfaces).

3.2. Land Cover Indices and LST Comparison

This study examined the relationship between land cover indices, urban index and LST. Surface reflectance (SR) and surface temperature (ST) data were used for analysis. Landsat LST measures the Earth's temperature in Kelvin. LST was converted to degrees Celsius using the Map Algebra toolset of Spatial Analyst Tools in ArcGIS Pro. The formula in Equation (1) applied for the conversion of LST from Kelvin to degrees Celsius is the following:

$$\begin{aligned} T(℃) &= T(\mathrm{K}) - 273.15 \\ &= LST \times 0.00341802 + 149 - 273.15 \end{aligned} \tag{1}$$

where T (°C) and T (K) are the LST in degrees Celsius and Kelvin, respectively. LST is the stored ST values in the Landsat Collection-2 data derived from band 6 for Landsat 5 and 7 and band 10 for Landsat 8, respectively. The 0.00341802 and 149 are the two linear coefficients used to convert the stored values to ST in Kelvin (K) (Christopher *et al*., 2023).

SR data were used to derive spectral indices. NDVI measures the reflectance of incoming solar radiation from the Earth's surface to the Landsat sensor. It is widely used to extract information about vegetation density, predict crop production, monitor drought, and measure surface temperature. In addition, NDVI measures vegetation abundance and is frequently used to indicate land surface characteristics in studies related to UHI.

The formula in Equation (2) used for NDVI index calculation of different wavelengths of the Landsat data is the following:

$$\begin{aligned} NDVI &= \frac{(NIR - Red)}{(NIR + Red)} \\ NDVI(Landsat\ 4,5\ \&\ 7) &= \frac{(Band\ 4 - Band\ 3)}{(Band\ 4 + Band\ 3)} \\ NDVI\ (Landsat\ 8\ \&\ 9) &= \frac{(Band\ 5 - Band\ 4)}{(Band\ 5 + Band\ 4)} \end{aligned} \tag{2}$$

where NDVI value always ranges from −1 to + 1.

NIR is the near-infrared waveband (band 4), and Red is the visible band (band 3). The NDVI value for green vegetation ranges from 0.1 to 0.7, so higher values indicate healthy and dense vegetation cover.

The two-band enhanced vegetation index (EVI2) was derived using the following formula in Equation (3):

$$EVI2 = \frac{2.5 * (NIR - Red)}{(NIR + Red + 1.0)} \tag{3}$$

where EVI2 value ranges from −1 to + 1.

UI was derived using the following formula, explained in Equation (4):

$$UI = \frac{(SWIR - NIR)}{(SWIR + NIR)} \tag{4}$$

where UI value ranges from −1 to + 1.

To evaluate the influence of land cover characteristics on land surface temperature, vegetation indices (NDVI, EVI2), UI, and LST were compared across multiple years. NDVI, EVI2, and UI were treated as

independent variables, while LST served as the dependent variable (Figure 6). Regression analysis was employed to quantify the bivariate relationships between LST and each land cover index.

Ordinary least squares and geographically weighted regression were used to estimate regression slopes and assess the strength of these relationships. OLS provided global estimates of the correlation, while GWR captured local variations in regression coefficients across the study area.

For statistical analysis, raster datasets of LST and land cover indices were converted into point features. A total of 800 random points were generated across the study area, and values of NDVI, EVI2, UI, and LST were extracted at these locations using the Extract by Mask tool in the Spatial Analyst extension of ArcGIS Pro. This approach ensured representative sampling of both urban and non-urban environments.

Scatterplot diagrams were generated from both OLS and GWR outputs to examine the bivariate correlations between land cover indices and LST for 1990, 2000, 2010, and 2020. While the OLS scatterplots reflected overall global trends rather than detailed spatial variation, the GWR scatterplots provided precise detail by capturing local differences and temporal changes in the strength of these relationships. Therefore, only the GWR scatterplots were presented in the paper (Figure 6), as they more effectively illustrate the spatial heterogeneity in the associations between vegetation indices, urban index, and LST. In the scatterplot, LST values illustrated the surface temperature gradient, NDVI, EVI2, and UI values reflected temporal variation in vegetation cover and urban development across the study area.

3.3. Quantifying UHI Intensity

The first step in calculating urban heat island intensity was to delineate the urban boundary. Urban areas identified in 2017 within the administrative boundary of Denver were defined as the extent of the urban core, based on the land cover dataset. To establish reference conditions, non-urban buffers extending 10 km beyond the urban boundary were generated. More than 99% of these buffer zones were classified as non-urban land cover types.

UHI intensity was then quantified as the temperature difference between urban and non-urban areas from 1990 to 2020. Specifically, LST values for each urban pixel (30 m resolution) were compared with the mean LST of surrounding non-urban buffer pixels. This approach allowed estimation of both temporal trends and spatial variation in UHI intensity across the study area. The calculation of UHI intensity followed the method outlined by Xian *et al*. (2021). The following formula has been used (see Equation (5)).

$$UHII\ (i) = Tu(i) - \overline{T}\,r(i) \tag{5}$$

Here, $UHII\ (i)$ is the UHI intensity for an urban pixel i, $Tu(i)$ is the temperature of the urban pixel i, and $\overline{T}\,r(i)$ is the mean LST of a surrounding non-urban buffer pixel i (Xian *et al*., 2021). The UHI intensities associated with different land cover types have been quantified, and new urban growth regions have been identified (Xian *et al*., 2021).

The Landsat-derived annual mean LST was used to quantify UHI intensity while minimizing the influence of short-term daily fluctuations. The annual mean LST was calculated following the algorithm developed by the USGS Earth Resources Observation and Science (EROS) center for UHI studies (Xian *et al*., 2021). This algorithm removes pixels contaminated by clouds, shadows, and snow/ice using the Landsat surface reflectance quality assessment (QA) and surface temperature quality assessment (STQA) bands. Clear-sky pixels with surface temperatures above 0 °C were averaged from March through November to reduce the influence of snow, ice, and cloud contamination (Xian *et al*., 2021). In this study, we adopted this approach by using pixels with effective seasonal records to compute annual mean LST values, which were then applied to analyze temporal changes in Denver's LST (1990–2020) and to generate UHI intensity maps.

4. Results and Discussion

4.1. Urban Land Cover Change Analysis

Seven of the eight land cover classes defined in the Land Change Monitoring, Assessment, and Projection (LCMAP) dataset were considered in this study; the permanent ice/snow class was excluded, as it is not present in the Denver metropolitan region. LCMAP was used to generate land cover maps for 1990, 2000, 2010, and 2020 (Figures 3a & 3d), allowing assessment of spatial patterns and temporal changes in land

cover over the 30 years. These maps were directly obtained from pre-classified LCMAP products, which are generated by the USGS using Landsat observations through an established processing and validation framework. For this study, the LCMAP data were subset to the Denver region, and the relevant classes were selected and visualized in ArcGIS Pro.

In 1990, grassland and shrubland dominated the southern and northwestern portions of the study area, while cropland was concentrated in the northeast. Urban development was largely confined to the central city (Figure 3a). By 2000, developed land cover had increased by approximately 7% relative to 1990, primarily through the conversion of grassland and cropland (Figure 3b). Expansion occurred to the north and south, with additional but more limited growth to the east and northwest. While some cropland persisted in the northeast, much of the grassland and shrubland in the south had already been converted to urban use (Figure 3b). By 2020, a substantial proportion of the cropland and grass/shrubland present in 1990 and 2000 had been replaced by developed land, reflecting extensive urban expansion across the study area (Figure 3d).

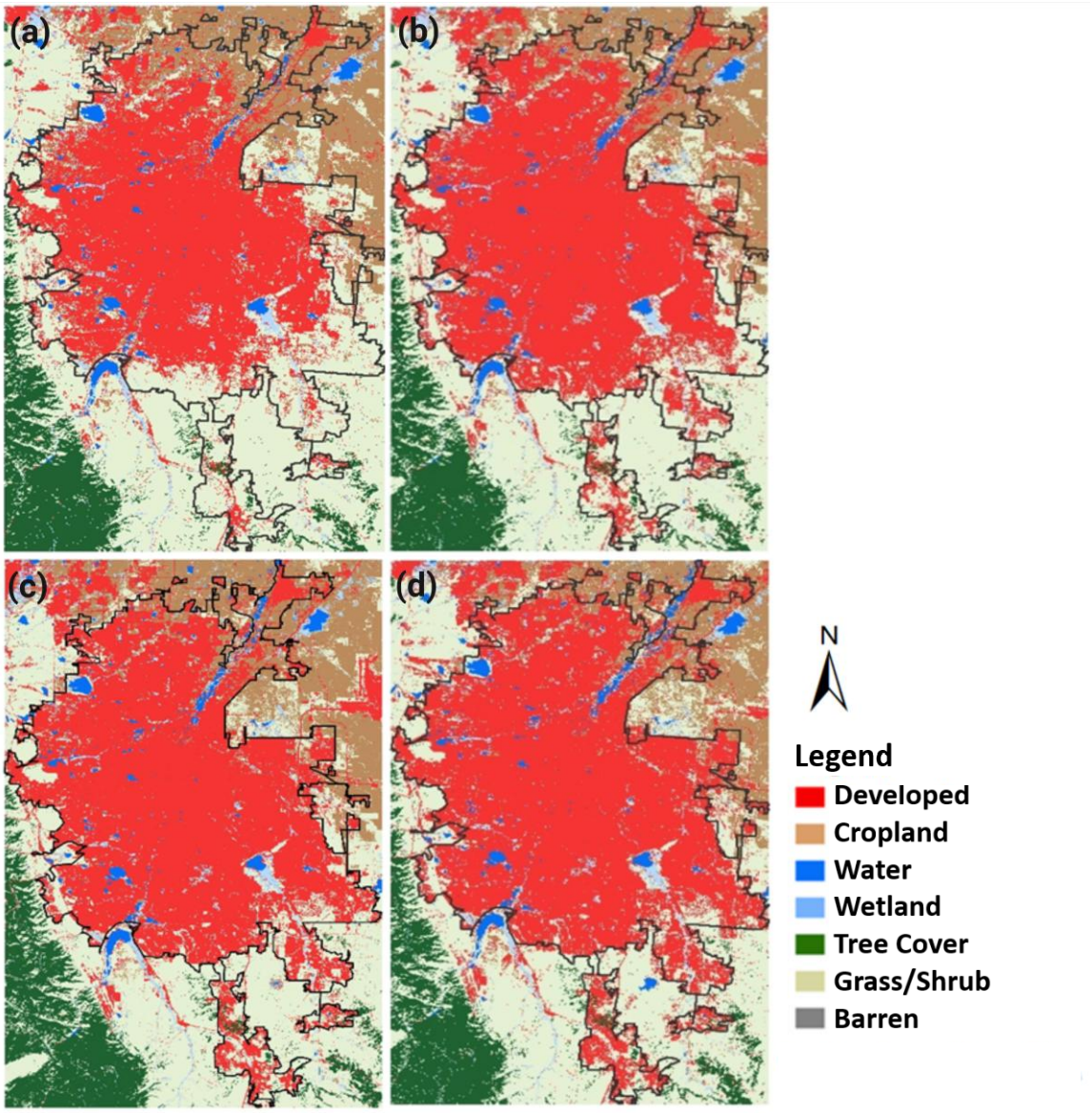

Figure 3. Land cover patterns and changes in Denver city in 1990 (a), 2000 (b), 2010 (c), and 2020 (d) with seven land cover classes.

4.2. Seasonal NDVI

NDVI values provide information about vegetation cover, abundance, and type across the landscape. Using Landsat reflectance data, NDVI maps were created for multiple years and three different seasons (Figures 4a–f). To highlight long-term trends, the comparison between 1990 and 2020 is emphasized, since it best illustrates landscape changes over three decades. Summer results were the most reliable, though fall and winter patterns were also considered. In urban areas, NDVI values were consistently low, reflecting limited vegetation and a high proportion of impervious surfaces. The lowest values were concentrated in the city center and commercial districts with dense development, while suburban areas retained slightly higher values. In contrast, the northeast and north-central parts of the city generally showed higher NDVI values across all years. In the city center, NDVI values during summer (June–August) ranged from 0.01 to 0.10 (Figures 4a & 4b). In fall (September–November), values ranged from 0.02 to 0.18 (Figures 4c & 4d), and in winter (December–February) from 0.001 to 0.10 in both 1990 and 2020 (Figures 4e & 4f). These values highlight the sharp contrast between heavily built-up urban zones and greener suburban or undeveloped areas.

Denver International Airport, located in the northeast of the city, had the lowest NDVI value (0.002), reflecting very little vegetation. In contrast, the western part of Denver, which includes mountain areas, showed much higher NDVI values due to dense vegetation. Figures 4a–d illustrate that the city center consistently had low NDVI values in both summer and fall, since this highly urbanized core is dominated by built-up surfaces. The western side of Denver changed very little between 1990 and 2020 because the mountains limited development. Instead, most urban expansion occurred in the northeast, while the southern part of the city experienced only minor changes. NDVI patterns outside the city were uneven, especially in winter, when NDVI is less reliable as an indicator of vegetation cover.

4.3. Seasonal LST

LST maps were created from Landsat data, with all values shown in degrees Celsius (Figures 5a−f). To show long-term change, we focus on 1990 and 2020 across summer, fall, and winter. Although data were also available for 2000 and 2010, the 1990–2020 comparison best captures the overall warming trend, and summer results were the most consistent across years.

Over the past 30 years, mean seasonal LST values rose sharply, especially in the urban core where new developments added more heat-absorbing surfaces. In 1990, seasonal mean LSTs were estimated at 7.8 °C in summer, 19.0 °C in fall, and −19.4 °C in winter in the Denver metropolitan area. By 2020, these values had increased substantially to 47.6 °C in summer, 34.9 °C in fall, and 11.4 °C in winter. This shows overall warming and a smaller seasonal gap compared to earlier decades. The unusually low winter average in 1990 and the relatively warm summer average in the same year are likely caused by residual effects of snow cover, incomplete masking of water surfaces, or atmospheric contamination in the remote sensing imagery, rather than by actual surface conditions.

Figure 5 depicts LST using a color gradient, where dark blue represents cooler areas and red indicates hotter areas. A comparison of the summer maps between 1990 and 2020 reveals a distinct shift in the central city from yellow to deep red, reflecting a substantial rise in surface temperatures. The steady increase in all seasons and a reduction of the seasonal difference evident that Denver has seen substantial surface warming, driven by land cover change and rapid urbanization. This increase corresponds to the expansion of impervious, built-up surfaces, which intensified the UHI effect.

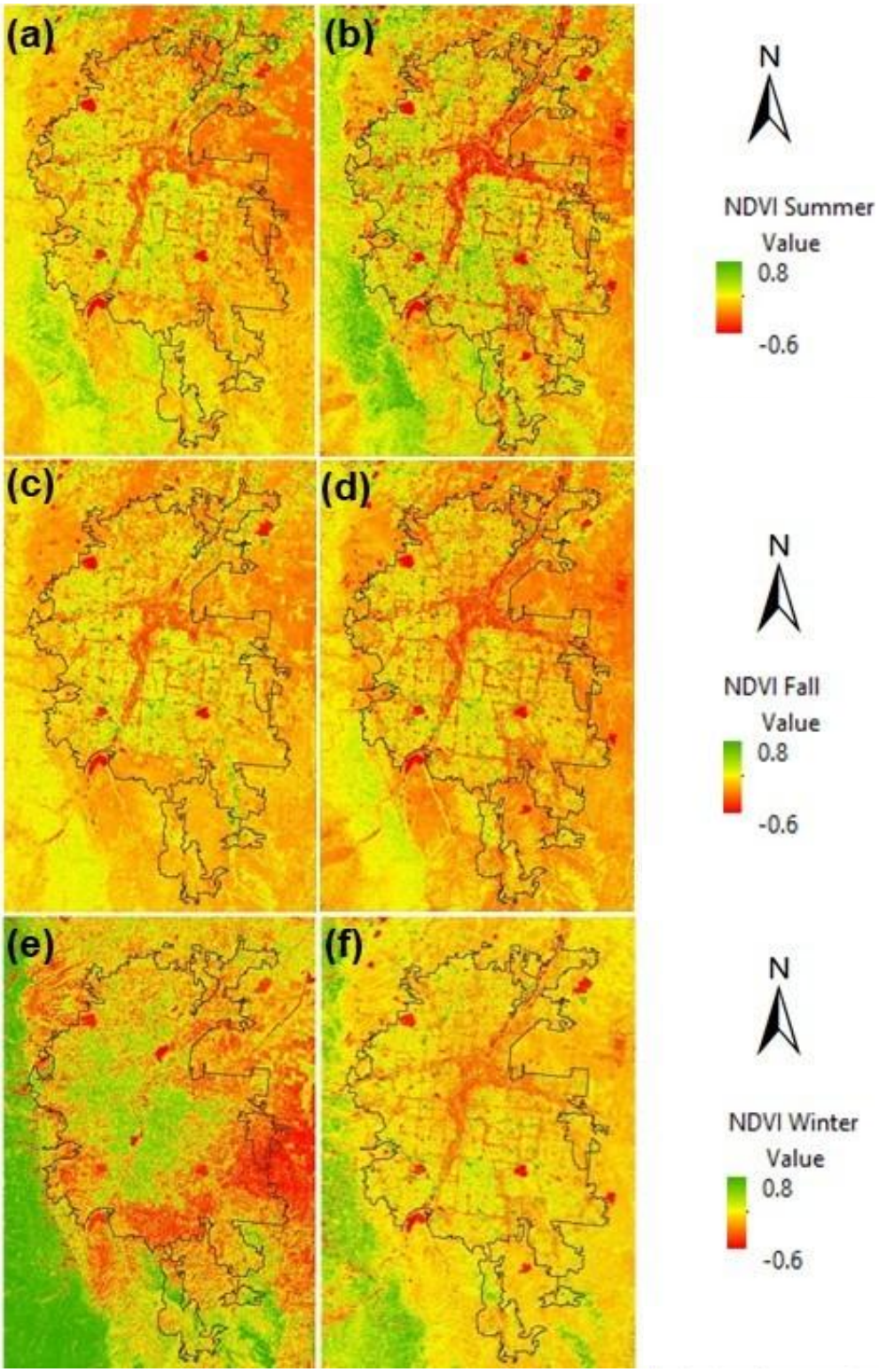

Figure 4. Spatial and temporal distribution of NDVI in the Denver urban area across three seasons, summer (a, b), fall (c, d), and winter (e, f)—for the years 1990 (a, c, e), and 2020 (b, d, f).

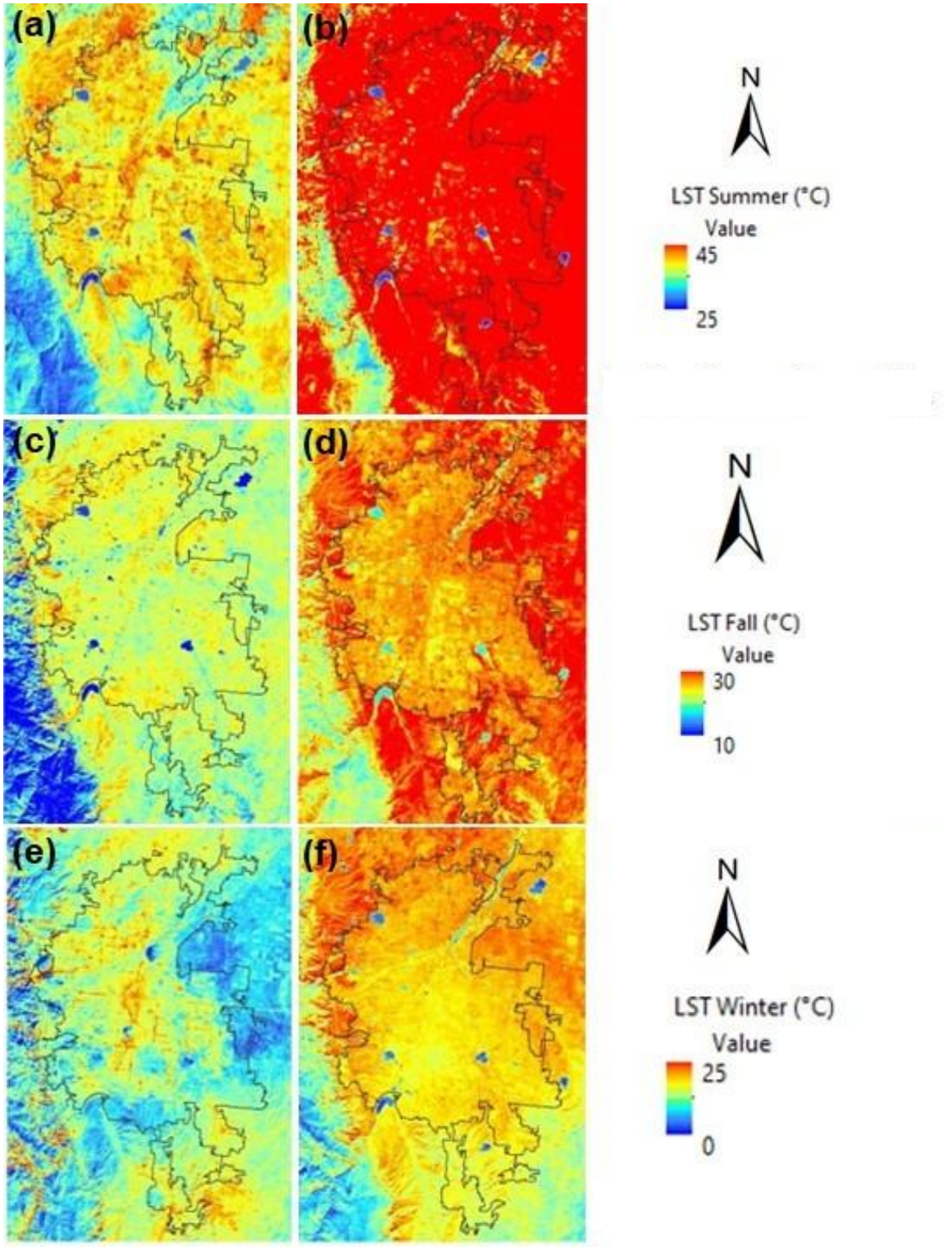

Figure 5. Spatial and temporal distribution of LST (°C) across three seasons—summer (a, b), fall (c, d), and winter (e, f)—for two reference years: 1990 (a, c, e), and 2020 (b, d, f) in the Denver urban area.

4.4. Relationship between Land Cover Indices and LST

The relationship between vegetation indices (NDVI, EVI2), the UI, and LST was analyzed using regression models. OLS regression provided the slope of these relationships, showing whether the correlation was negative (e.g., more vegetation linked to cooler temperatures) or positive (e.g., more built-up land linked to hotter temperatures). Figure 6 includes scatter plots from the GWR model, which illustrates how well the predicted values match the observed data.

To measure the strength of these relationships, we used the R^2 statistic. This value, which ranges from 0 to 1 (or 0% to 100%), indicates how much of the variation in LST can be explained by the independent variables (NDVI, EVI2, and UI). An R^2 of 1.0 means a perfect fit, while a value near 0 means the variables do not explain LST well.

However, relying solely on R^2 for interpretation can be misleading. A low R^2 does not necessarily mean the model is poor, nor does a high R^2 always mean it is ideal. Scatter plots may reveal biases or mismatches between data points and model predictions. Thus, R^2 is best seen as one indicator of how well the model captures the relationship between land cover indices and LST (Kutner *et al*., 2004)

The OLS regression analysis showed how strongly land cover and urban indices (NDVI, EVI2, and UI) were related to LST in Denver for 1990, 2000, 2010, and 2020. For the UI, the adjusted R^2 was 3% in 1990, indicating a weak relationship with LST. By 2000, the relationship strengthened considerably (42%) but then declined in 2010 (14%) before rising again in 2020 (32%). For the EVI2, the adjusted R^2 was 8% in 1990, increased to 25% in 2000, dropped slightly to 15% in 2010, and settled at 18% in 2020. These results suggest that the influence of built-up areas and vegetation on LST varied over time, with the strongest relationships occurring around 2000, followed by weaker correlations in 2010, and increasing again by 2020.

The OLS model did not represent the spatial heterogeneity within the study area, although it offered a helpful global summary of these associations. To overcome these limitations, GWR was then applied to examine how NDVI, EVI2, and UI related to LST in Denver for 1990, 2000, 2010, and 2020. The results showed relatively low adjusted R^2 values in 1990, meaning the land cover indices explained only a small portion of the variation in LST at that time. Nevertheless, the analysis confirmed that NDVI, EVI2, and UI influence LST. While these indices are not the only factors affecting surface temperature, they also contribute to its changes. This supports the study's goal of identifying how land cover characteristics are linked to variations in LST.

Figure 6 presents scatter plots from the GWR model, showing how NDVI, EVI2, and UI explained variations in land surface temperature across four time periods. For NDVI, the adjusted R^2 was 8% in 1990, increased to 25% in 2000, then declined to 15% in 2010, and rose slightly to 18% in 2020. The urban index showed the lowest value in 1990 at 3%, but it climbed sharply to 43% in 2000 before dropping to 14% in 2010 and recovering to 32% in 2020. For EVI2, the adjusted R^2 was 8% in 1990, rose to 26% in 2000, fell sharply to 3% in 2010, and improved to 19% in 2020. According to the literature, adjusted R^2 values between 10% and 50% are generally acceptable when statistically significant (Fricker *et al*., 2015). The results of this study fall within that range, confirming that vegetation and urban indices had a meaningful, though varying, influence on LST across the three decades. Overall, UI generally showed the strongest influence on surface temperature, while NDVI and EVI2 played smaller but more consistent roles.

The correlation between vegetation indices and LST follows a consistent trend: as NDVI and EVI2 increase, LST decreases, and vice versa. Increased vegetation cover is associated with a reduction in the slope of temperature change, whereas vegetation loss corresponds to an increase in that slope. In contrast, the expansion of developed and built-up land cover contributes to substantial increases in temperature. The relationships among NDVI, EVI2, the urban index, and LST are influenced by seasonal variation, diurnal cycles, and data accuracy. The negative correlation between NDVI/EVI2 and LST is largely attributable to vegetation density and the topographic characteristics of the study area. Overall, these relationships remain consistent across all years examined. Previous research has demonstrated that the NDVI–LST relationship is particularly pronounced and reliable during summer months. In this study, linear regression analysis was applied using NDVI, EVI2, and UI as explanatory variables to quantify their bivariate correlations with LST.

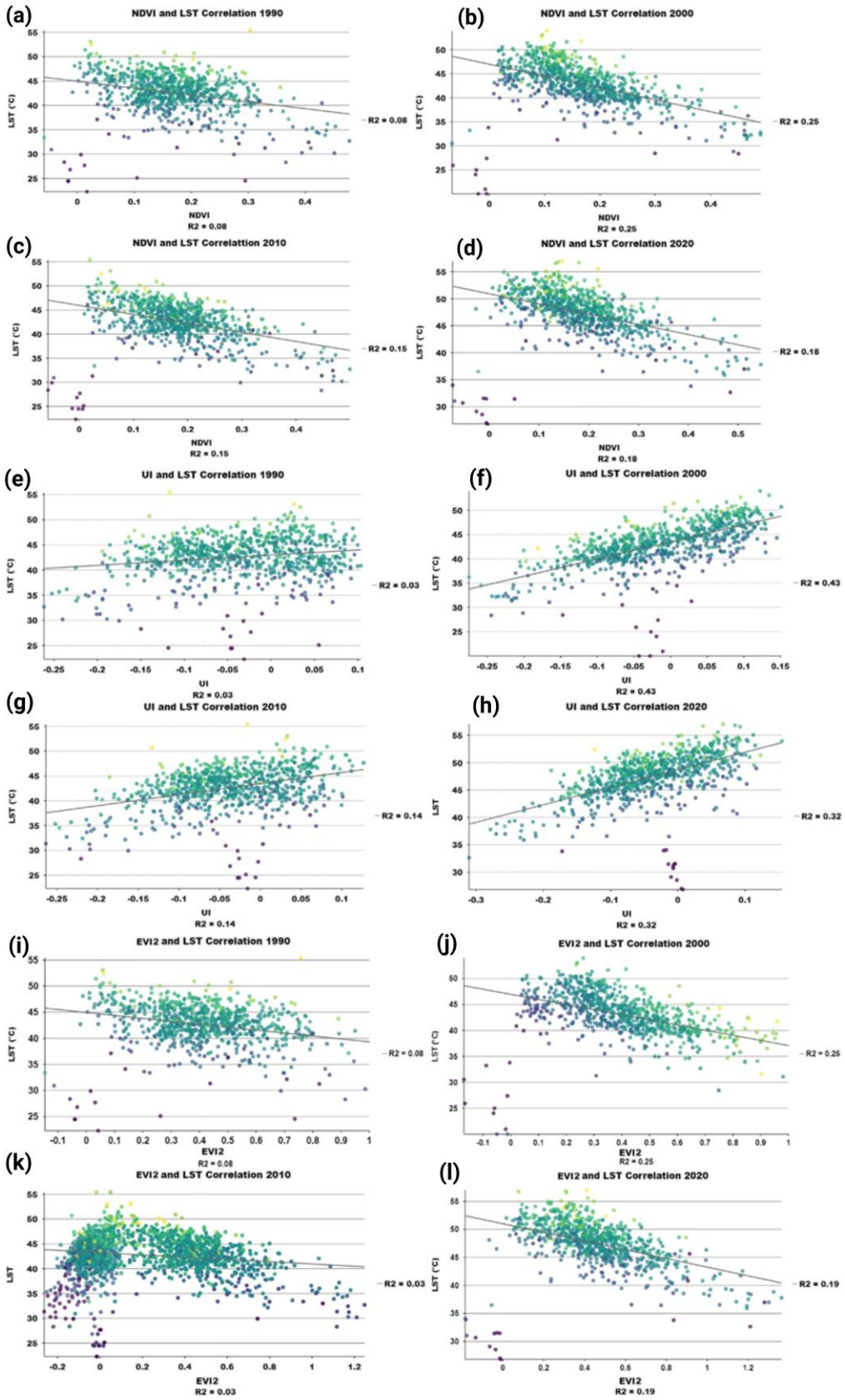

Figure 6. Geographically weighted regression analysis between NDVI, EVI2, UI, and LST (°C) in the Denver urban area in four different years (1990, 2000, 2010, and 2020) depicts the trend of correlation between land cover and LST.

4.5. UHI Intensity

4.5.1. Mean Annual LST

Figure 7 shows the annual mean LST, highlighting the spatial distribution of surface temperatures across Denver and its surrounding 5 km and 10 km non-urban buffers. The results reveal a pronounced urban–rural temperature gradient, with consistently higher LST values in urban areas relative to adjacent non-urban zones between 1990 and 2020. By 2020, LSTs were substantially elevated within Denver, particularly in the northeastern sector of the 5 km buffer, where urban expansion contributed to localized warming (Figure 7c). The most pronounced hotspots were located in downtown Denver, the central business district, major commercial zones, and the airport area in the northeast.

In 1990, the mean LST in Denver was 23 °C (Figure 7a), with increased temperatures concentrated in the northeastern areas, particularly in built-up areas such as the airport and commercial zones. By 2000, the mean LST had increased to 24 °C, with higher values observed across the northern, northeastern, southern, and southeastern parts of the city (Figure 7b). These patterns indicate that urban development was closely associated with localized warming. In 2010, the mean LST rose further to 26 °C (Figure 7c), and by 2020, the mean LST had reached 28 °C (Figure 7d), reflecting a significant increase relative to 1990 and 2000 (Figure 7d). Overall, the results highlight a steady rise in LST over three decades, with rapid changes occurring in the most recent decade. These patterns strongly suggest that Denver has undergone pronounced surface warming, linked to rapid urban expansion and associated land cover transformations. Furthermore, the gradual increase in annual mean LST from 23 °C in 1990 to 28 °C in 2020 supports the warming trend while reducing the influence of seasonal anomalies.

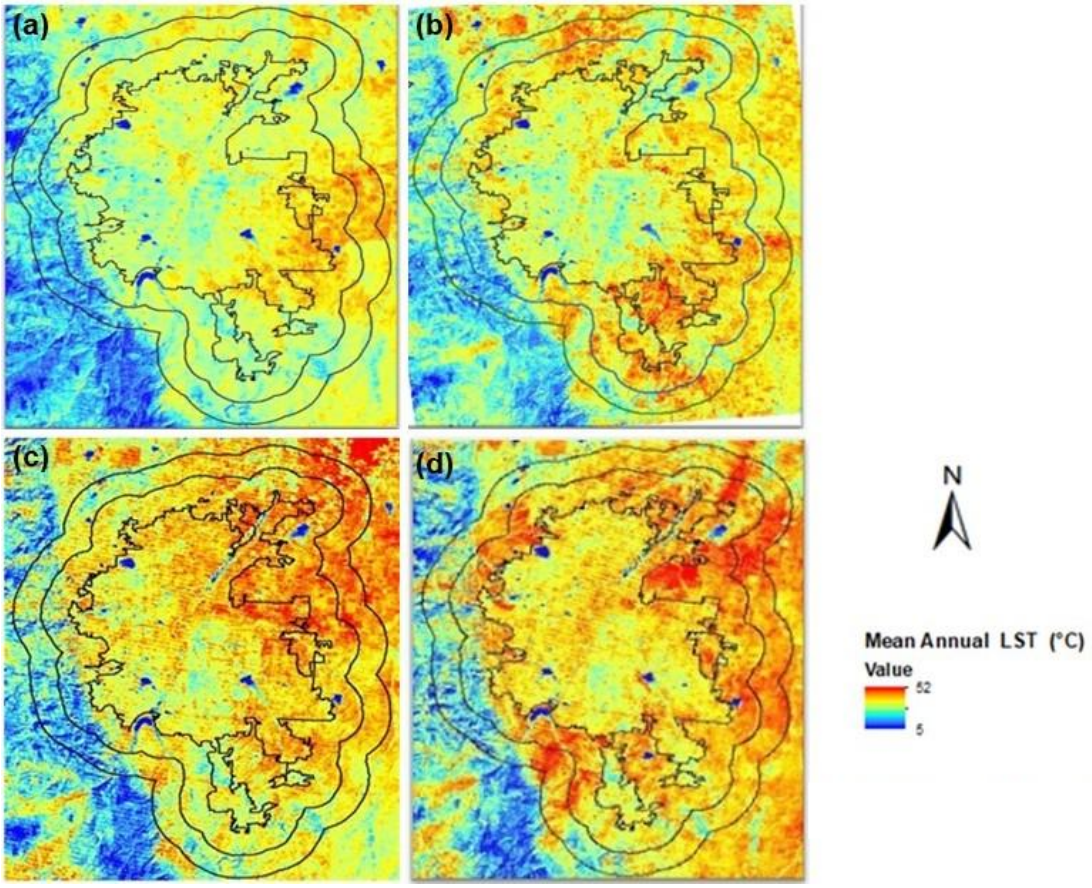

Figure 7. Mean annual LST (°C) in Denver in 1990 (a), 2000 (b), 2010 (c), and 2020 (d).

The spatial distribution of LST is characterized by elevated values in urbanized areas, including industrial zones, downtown districts, and the airport. However, beginning in 2003, the Landsat 7 Scan Line Corrector (SLC) malfunction introduced data gaps that produced artificial striping in the imagery, leading to

anomalously low LST estimates in both urban and rural areas (Xian *et al*., 2021). These artifacts are evident in the mean LST maps for 2010 and 2020 (Figures 7c & 7d), where stripes of lower temperature values appear across the study area. Consequently, the estimation of mean LST for these years may be partially affected by SLC-related errors, as reflected in the striping patterns observed in the LST difference maps (Xian *et al*., 2021).

4.5.2. Annual UHI Intensity

Urban heat island intensity in Denver was quantified by comparing the land surface temperature of urban pixels with the mean LST of surrounding non-urban buffer zones extending 10 km from the city boundary. Specifically, UHI intensity was calculated as the difference between the LST of each urban pixel and the mean LST of the corresponding 10 km non-urban buffer. Mean annual LST values from 1990, 2000, 2010, and 2020 were used to assess temporal and spatial trends in UHI intensity (Figures 8a–d).

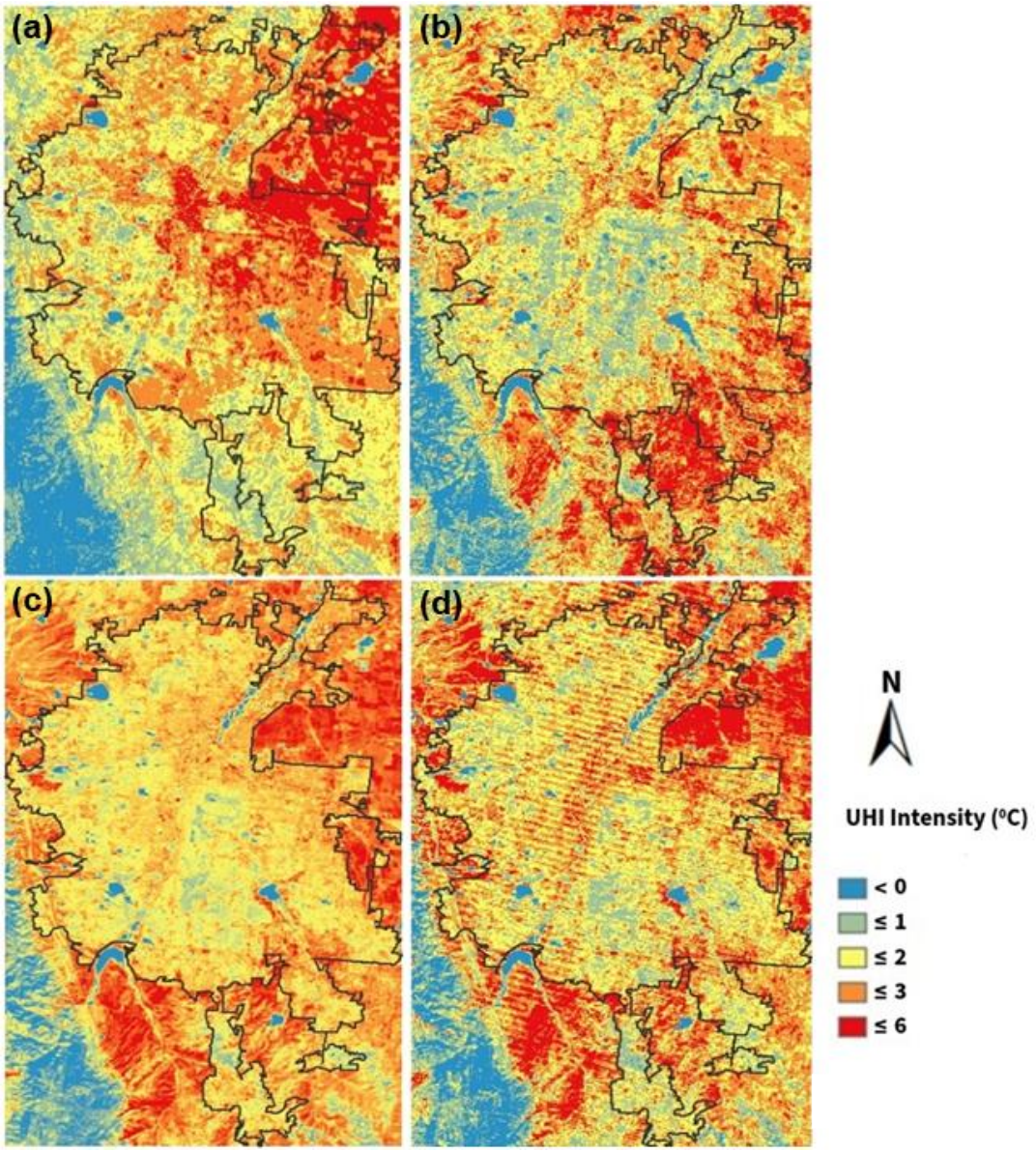

Figure 8. Spatial and temporal distribution of annual UHII (Degree Celsius) in 1990 (a), 2000 (b), 2010 (c), and 2020 (d), and temporal trends of change in UHII from 1990 to 2020.

In 1990, the mean annual UHI intensity was –1.5 °C (Figure 8a). Spatial patterns revealed higher UHI intensity in the northeastern portion of the city, moderate intensity in the southeastern and south-central areas,

and relatively low intensity in the southwest. These results highlight the heterogeneous nature of UHI intensity across Denver's urban landscape.

In 2000, the mean annual UHI intensity was –0.89 °C (Figure 8b), reflecting a shift in spatial distribution compared to 1990 (Figure 8a). The highest UHI intensity values were concentrated in the southeastern and southwestern parts of Denver, while moderate values appeared in the northern, northeastern, and northwestern portions of the city. These patterns suggest that by 2000, UHI effects had become more spatially dispersed across both urban and adjacent rural areas within the 10 km buffer.

By 2020, the mean annual UHI intensity had increased to 1 °C (Figure 8d). The UHI map indicates substantial changes in the northeastern sector of Denver relative to 2000, coinciding with continued urban expansion. Similar to 2000, higher to moderate UHI intensity values persisted in the southeastern portion of the study area (Figures 8c & 8d). These results highlight both the intensification and redistribution of UHI effects over time, with notable growth in magnitude and spatial extent between 2000 and 2020.

The UHI intensity maps (Figures 8a–d) illustrate the spatial distribution and temporal evolution of UHI intensity in Denver over the past three decades. The results derived from mean annual LST indicate that changes in UHI intensity were not uniform across time but showed a general increasing trend. Spatial patterns varied, with some areas exhibiting scattered distributions of UHI intensity, while others displayed more concentrated hotspots within and beyond the urban boundary. Shifts in land cover and modifications to the thermal environment strongly influenced these patterns. For instance, large-scale developments such as the expansion of Denver International Airport and the growth of Commerce City likely contributed to localized increases and redistribution of UHI intensity.

5. Future Work and Limitations

A primary limitation of this study lies in the method used to estimate UHI intensity, which was calculated as the difference between the temperature of urban pixels and the mean LST of non-urban buffer zones. The choice of buffer distance directly influences UHI estimates, as demonstrated in previous research. Xian *et al*. (2021) noted that UHI intensity depends on the spatial extent of selected urban and rural zones as well as the landscape characteristics of the study region. Similarly, Li *et al*. (2019) found that the size of the surrounding non-urban area strongly affects UHI estimation. Jiameng *et al*. (2018) reported that most remote-sensing-based studies use buffer widths ranging from 1 to 50 km to delineate non-urban extents. Although Xian *et al*. (2021) observed similar temporal trends in UHI intensity when using 5 km and 10 km buffers, there is currently no consistent standard for defining non-urban reference areas.

The results of this study further demonstrate the complexity of UHI estimation in Denver. For example, some areas outside the city exhibited higher UHI intensity than the urban core (Figure 8). This pattern reflects Denver's unique geographic and climatic context, including its semi-arid environment. On the eastern side of the city, sparse shrubland and bare soils—characterized by low heat absorption capacity—heat rapidly during the daytime, producing localized cooling contrasts that complicate UHI interpretation. Additionally, highly impervious zones such as Denver International Airport, located northeast of the city, generated higher LST than many urbanized portions of Denver itself. These examples underscore the localized nature of UHI, which varies with geographic setting, climate, land cover, and the composition of built-up surfaces. Consequently, UHI intensity should be analyzed with explicit consideration of local landscape characteristics, and future studies must account for the unique climatic and geographic conditions of each study area.

Future work should also incorporate additional biophysical and land cover variables to refine UHI estimation. Vegetation indices such as NDVI and EVI, while widely used, have notable limitations: NDVI saturates in high-biomass regions and is sensitive to background brightness in sparsely vegetated areas, whereas EVI is more stable across biomes but influenced by topographic factors (Huete *et al*., 2002; Matsushita *et al*., 2007; Reygadas *et al.,* 2020). The leaf area index (LAI) has been suggested as a complementary metric to overcome these shortcomings (Reygadas *et al.,* 2020). Similarly, tree canopy percentage is a strong predictor of LST, particularly from spring through fall (Decheng *et al*., 2014). Incorporating variables such as LAI, canopy cover, and impervious surface fraction into multivariate regression models can improve explanatory power by capturing more of the complex relationships driving LST variation. High-resolution land cover data would further enhance this capacity. For example, differentiating impervious surfaces into pavement and buildings, or separating vegetation into tree and grass classes, could yield more accurate predictions of LST.

Finally, future studies should explore the temporal dynamics of urban cooling in Denver, examining when and under what conditions cooling effects occur. Such analyses would help clarify the role of vegetation, land

cover, and microclimatic factors in shaping UHI patterns, and would contribute to more effective urban planning and climate adaptation strategies.

6. Conclusions

This study examined the relationships between land cover change, land surface temperature, and the spatial and temporal dynamics of urban heat island intensity in Denver using Landsat data from 1990 to 2020. The results highlight the significant impacts of rapid urbanization on surface thermal patterns and UHI intensity. Key findings include:

(1) Land cover change: Between 1990 and 2020, Denver experienced a 13% increase in developed land, primarily at the expense of cropland and grass/shrub cover, particularly in the southern and northeastern regions. These changes reflect substantial urban expansion over the study period.
(2) LST–land cover relationships: Linear and geographically weighted regression analyses revealed a consistent inverse relationship between vegetation indices (NDVI and EVI2) and LST, while the urban index exhibited a positive correlation. Adjusted R^2 values ranged from 0.03 to 0.43 across the study period, indicating variable explanatory power depending on year and spatial context.
(3) Temperature trends: The mean annual LST in Denver increased from 23 °C in 1990 to 28 °C in 2020. Higher temperatures were consistently concentrated in built-up areas, including downtown, commercial districts, and Denver International Airport.
(4) UHI intensity: Annual UHI intensity increased from –1.5 °C in 1990 to 1 °C in 2020. Spatial patterns revealed the emergence of concentrated hotspots in the northeastern and southeastern sectors of the city, as well as around the airport, coinciding with urban expansion.
(5) Methodological considerations: While NDVI, EVI2, and UI were significantly correlated with LST, other biophysical and atmospheric factors likely influence surface temperature. Incorporating additional metrics, such as the leaf area index (LAI) or detailed measures of impervious and vegetation cover, could enhance the explanatory capacity of future models.

Overall, this study demonstrates that urbanization has intensified LST and UHI effects in Denver over the past three decades. Findings underscore the strong link between rapid land cover transformation and intensification of UHI effects in the Denver metropolitan region. These findings provide a scientific basis for understanding UHI processes in rapidly growing cities and can inform urban planning and environmental management strategies aimed at mitigating heat-related impacts and enhancing urban sustainability.

Funding: This research received no specific grant from any funding agency in the public, commercial, or not-for-profit sectors.

Acknowledgment: We gratefully acknowledge their ongoing efforts to promote the use of remote sensing and geospatial technologies in scientific research and education. We would like to extend our gratitude to Dr. Hankui Zhang for his technical support and help with data acquisition, to Dr. Maitiniyazi Maimaitijiang and Dr. Kimberly Johnson Maier for their writing assistance, and to Dr. Hua Shi, Research Scientist at USGS EROS, for supplying the mean annual LST data used in this study.

Conflicts of Interest: The authors declare no conflicts of interest. The funders had no role in the study's design, the collection, analyses, or interpretation of data, the writing of the manuscript, or the decision to publish the results.

References

Aguiar, R.O.M., Gonçalves, H. (2002). Climate change impacts on the thermal performance of Portuguese buildings: Results of the SIAM study. *Building Services Engineering Research and Technology*, 23, 223–231. https://doi.org/10.1191/0143624402bt045oa

Anderson, J., Hardy, E., Roach, J., Witmer, R. (1976). A land use and land cover classification system for use with remote sensing data. *U.S. Geological Survey Professional Paper*, 964.

Buyantuyev, Alexander, & Wu, J. (2010). Urban heat islands and landscape heterogeneity: linking spatiotemporal variations in surface temperatures to land-cover and socioeconomic patterns. *Landscape Ecology*, 17-33. https://doi.org/10.1007/s10980-009-9402-4

Cao, Xin, Akio, O., Jin, C., & Hidefumi, I. (2010). Quantifying the cool island intensity of urban parks using ASTER and IKONOS data. *Landscape and Urban Planning* , 224-231.

Clinton, N., & Gong, P. (2013). MODIS detected surface urban heat islands and sinks: Global locations and controls. *Remote Sensing of Environment*(134), 294-304. https://doi.org/10.1016/j.rse.2013.03.008

Christopher, J. C., David, P. R., Saeed, A., Christopher, B., Eric, V., Glynn, H., Aaron, G., Mike, C., Christopher, E., Esad, M., Gail, S., Cody, A., Martha, A., Michelle, B., Bruce, C., Ray, D., Danny, H., Calli, J., Steve, Z. (2023). The 50-year Landsat Collection 2 archive. *Science of Remote Sensing*, 8, 100103. https://doi.org/10.1016/j.srs.2023.100103

Davis, R., 2021. Climate report: Denver's 'heat island' could get hotter and harder for homeless. *The Denver VOICE*, August 29, 2021. https://www.denvervoice.org/archive/2021/8/30/climate-report-denvers-heat-island-could-get-hotter-and-harder-for-homeless Last access: 30 June 2025.

Decheng, Z., Shuqing, Z., Shuguang, L., Liangxia, Z., Chao, Z. (2014). Surface urban heat island in China's 32 major cities: Spatial patterns and drivers. *Remote Sensing of Environment*, 152, 51–61. https://doi.org/10.1016/j.rse.2014.05.017

Dwyer, J.L., Roy, D.P., Sauer, B., Jenkerson, C.B., Zhang, H.K., Lymburner, L. (2018). Analysis Ready Data: Enabling analysis of the Landsat archive. *Remote Sensing*, 10, 1363. https://doi.org/10.3390/rs10091363

Frey, C. M., Rigo, G., & Parlow, E. (2007). Urban radiation balance of two coastal cities in a hot and dry environment. *International Journal of Remote Sensing*, 2695-2712. https://doi.org/10.1080/01431160600993389

Fricker, G.A., Wolf, J.A., Saatchi, S.S., Gillespie, T.W. (2015). Predicting spatial variations of tree species richness in tropical forests from high-resolution remote sensing. Ecological Applications, 25, 1776–1789. https://doi.org/10.1890/14-1593.1

George, X., Hua, S., Qiang, Z., Roger, A., Kevin, G., Zhuoting, W., Michael, K. (2022). Monitoring and characterizing multi-decadal variations of urban thermal condition using time-series thermal remote sensing and dynamic land cover data. *Remote Sensing of Environment*, 269, 112803. https://doi.org/10.1016/j.rse.2021.112803

Harald, Z., Ludwig, G., Luis, I. (2020). And the winner is? Comparing urban green space provision and accessibility in eight European metropolitan areas using a spatially explicit approach. *Urban Forestry & Urban Greening*, 49, 126603. https://doi.org/10.1016/j.ufug.2019.126603

Homer, C., Dewitz, J., Jin, S., Xian, G., Costello, C., Danielson, P., Gass, L., Funk, M., Wickham, J., Stehman, S., Auch, R., Riitters, K. (2020). Conterminous United States land cover change patterns 2001–2016 from the 2016 National Land Cover Database. *ISPRS Journal of Photogrammetry and Remote Sensing*, 162, 184–199.

Huete, A., Didan, K., Miura, T., Rodriguez, E.P., Gao, X., Ferreira, L.G. (2002). Overview of the radiometric and biophysical performance of the MODIS vegetation indices. *Remote Sensing of Environment*, 83, 195–213. https://doi.org/10.1016/S0034-4257(02)00096-2

Imhoff, L, M., Zhang, P., E, R., Wolfe, & Bounouaa, L. (2010). Remote sensing of the urban heat island effect across biomes in the continental USA. *Remote Sensing of Environment*, 504-513. https://doi.org/10.1016/j.rse.2009.10.008

Jiameng, L., Wenfeng, Z., Fan, H., James, V., Benjamin, B., Michael, A., Shushi, P., Falu, H., Yongxue, L., Peijun, D. (2018). Identification of typical diurnal patterns for clear-sky climatology of surface urban heat islands. *Remote Sensing of Environment*, 217, 203–220. https://doi.org/10.1016/j.rse.2018.08.031

Kenward, A., Yawitz, D., Sanford, T., Wang, R. (2014). *Summer in the city: Hot and getting hotter*. Climate Central Report.

Keyvan, E., Manouchehr, C., Mohsen, A., Ali Akbar, M. (2021). Spatiotemporal analysis of land surface temperature using multi-temporal and multi-sensor image fusion techniques. *Sustainable Cities and Society*, 64, 102508. https://doi.org/10.1016/j.scs.2020.102508

Kutner, M.H., Nachtsheim, C.J., Neter, J., 2004. *Applied Linear Regression Models*, 4th ed. McGraw-Hill/Irwin, New York.

Li, K., Chen, Y., Wang, M., Gong, A. (2019). Spatial–temporal variations of surface urban heat island intensity induced by different definitions of rural extents in China. *Science of the Total Environment*, 669, 229–247. https://doi.org/10.1016/j.scitotenv.2019.02.408

Liu, H., Weng, Q. (2009). Scaling effect on the relationship between landscape pattern and land surface temperature: A case study of Indianapolis, United States. *Photogrammetric Engineering and Remote Sensing*, 75, 291–304.

Matsushita, B., Yang, W., Chen, J., Onda, Y., Qiu, G. (2007). Sensitivity of the Enhanced Vegetation Index (EVI) and Normalized Difference Vegetation Index (NDVI) to topographic effects: A case study in high-density cypress forest. *Sensors*, 7, 2636–2651. https://doi.org/10.3390/s7112636

MRLC. (2016). MRLC Evaluation Report. https://www.mrlc.gov/ Last access: 20 June 2025.

Peng, J., Jia, J., Liu, Y., Li, H., & Wu, J. (2018). Seasonal contrast of the dominant factors for spatial distribution of land surface temperature in urban areas. *Remote Sensing of Environment, 215*, 255–267. https://doi.org/10.1016/j.rse.2018.06.010

Reygadas, Y., Jensen, J. L., Moisen, G. G., Currit, N., & Chow, E. T. (2020). Assessing the relationship between vegetation greenness and surface temperature through Granger causality and impulse-response coefficients: A case study in Mexico.

International Journal of Remote Sensing, 41, 3761–3783. https://doi.org/10.1080/01431161.2019.1711241

Richard, L.-R., Luis, I., Harald, Z. (2022). Intraurban heterogeneity of space–time land surface temperature trends in six climate-diverse cities. *Science of the Total Environment*, 804, 150037. https://doi.org/10.1016/j.scitotenv.2021.150037

Stephen, V.S., Bruce, W.P., Josephine, A.H., Danika, F.W. (2021). Validation of the U.S. Geological Survey's Land Change Monitoring, Assessment and Projection (LCMAP) Collection 1.0 annual land cover products 1985–2017. *Remote Sensing of Environment*, 265, 112646. https://doi.org/10.1016/j.rse.2021.112646

Streutker, D.R. (2002). A remote sensing study of the urban heat island of Houston, Texas. *International Journal of Remote Sensing*, 23, 2595–2608. https://doi.org/10.1080/01431160110115023

United Nations. (2018). *World Urbanization Prospects: The 2018 Revision*. UN Department of Economic and Social Affairs, New York.

Voogt, J.A., Oke, T.R. (2003). Thermal remote sensing of urban climates. *Remote Sensing of Environment*, 86, 370–384. https://doi.org/10.1016/S0034-4257(03)00079-8

Weng, Q., Lu, D., Liang, B. (2006). Urban surface biophysical descriptors and land surface temperature variations. *Photogrammetric Engineering & Remote Sensing*, 72, 1275–1286. https://doi.org/10.14358/PERS.72.11.1275

World Report. (2019). *World Report.* Retrieved from https://www.hrw.org/world-report/2019

Xian, G. (2008). Satellite Remotely-sensed Land Surface Parameters and Their Climatic Effects for Three Metropolitan Regions. *Advances in Space Research*(41), 1861-1869. https://doi.org/10.1016/j.asr.2007.11.004

Xian, G., Shi, H., Auch, R., Gallo, K., Zhou, Q., Wu, Z. (2021). The effects of urban land cover dynamics on urban heat island intensity and temporal trends. *GIScience & Remote Sensing*, 58, 501–515. https://doi.org/10.1080/15481603.2021.1903282

Yue, W., Xu, J., Tan, W., & Xu, L. (2007). The relationship between land surface temperature and NDVI with remote sensing: application to Shanghai Landsat 7 ETM+ data. International Journal of Remote Sensing, 28(15), 3205–3226. https://doi.org/10.1080/01431160500306906

Yuvaraj, R.M. (2020). Extents of predictors for land surface temperature using multiple regression model. *The Scientific World Journal*, 2020, 3958589. https://doi.org/10.1155/2020/3958589

Zhengming, W., Dozier, J. (1996). A generalized split-window algorithm for retrieving land-surface temperature from space. *IEEE Transactions on Geoscience and Remote Sensing*, 34, 892–905. https://doi.org/10.1109/36.508406